5466–5476 Nucleic Acids Research, 1994, Vol. 22, No. 24

Crystal structure of the highly distorted chimeric decamer r(C)d(CGGCGCCG)r(G)·spermine complex — spermine binding to phosphate only and minor groove tertiary base-pairing

Changill Ban, B.Ramakrishnan and M.Sundaralingam*
Biological Macromolecular Structure, Departments of Chemistry and Biochemistry, The Ohio State University, 1060 Carmack Road, Columbus, OH 43210, USA

Received June 29, 1994; Revised and Accepted October 21, 1994

ABSTRACT

The crystal structure of the self-complementary chimeric decamer duplex r(C)d(CGGCGCCG)r(G), with RNA base pairs at both termini, has been solved at 1.9 Å resolution by the molecular replacement method and refined to an R value of 0.145 for 2,314 reflections. The C3′-*endo* sugar puckers of the terminal riboses apparently drive the entire chimeric duplex into an A-DNA conformation, in contrast to the B-DNA conformation adopted by the all-deoxy decamer of the same sequence. Five symmetry related duplexes encapsulate a spermine molecule which interacts with ten phosphate groups, both directly and through water molecules to form multiple ionic and hydrogen bonding interactions. The spermine interaction severely bends the duplexes by 31° into the major groove at the fourth base pair G(4)·C(17), jolts it and slides the 'base plate' into the minor groove. This base pair, together with the adjacent base pair in the top half and the corresponding pseudo two-fold related base pairs in the bottom half, form four minor groove base-paired multiples with the terminal base pairs of two neighboring duplexes.

INTRODUCTION

In our investigations on the conformation of the Okazaki fragment, where a short RNA primer initiates DNA replication, we previously introduced a single ribose in the center of the decamer, d(CCGGC)r(G)d(CCGG) (1) (here after called chimer-1), and found that it converted the all-deoxy B-DNA decamer of the same base sequence (2) to A-DNA/RNA. In the present study we have introduced riboses at either termini of the decamer, r(C)d(CGGCGCCG)r(G) (RNA–DNA–RNA), and find that the duplex is again converted to A-DNA where all the eight inner deoxy riboses also adopt the C3′-*endo* puckering preferred by the terminal riboses.

The polycationic spermine is generally used in oligonucleotide crystallization, but it is usually disordered in the bulk solvent and seldom found in electron density maps. A well ordered spermine molecule is found in this A-DNA crystal, interacting only with the phosphate groups of five neighboring duplexes. This is in contrast to base only (3) or both the base and phosphate group (4) interactions in other A-DNA structures. In the B-DNA–drug complexes (5, 6) and Z-DNA (7, 8), both the base and phosphate groups interact with spermine. Polyamines like spermine are often found in large amounts in eukaryotic cells and viruses. These amines are biologically important in the packaging of chromatin DNA, but their exact roles are not fully understood. By analogy with the histone proteins, which have numerous positively charged lysine and arginine residues, spermine may be expected to serve a similar function, neutralizing the negatively charged phosphate groups and playing a role in DNA packaging.

METHODS AND MATERIALS

Synthesis, crystallization and data collection

The chimeric decamer r(C)d(CGGCGCCG)r(G) was synthesized and purified as done previously (1). The crystallization was carried out by the hanging drop vapor diffusion method in the presence of 1 mM decamer r(C)d(CGGCGCCG)r(G) (single strand concentration), 40 mM sodium cacodylate buffer (pH 7.0) and 2.0 mM spermine tetrachloride against 45% 2-methyl-2,4-pentanediol (MPD). Small crystals appeared in three days which grew to dimensions of 0.2mm×0.2mm×0.2mm in a week. A single crystal was mounted in an arbitrary orientation in a 0.5mm Lindemann glass capillary with some mother liquid at one end. Even though the crystal diffracted to 1.9 Å resolution, the diffraction showed a high mosaic pattern and posed difficulty in indexing the data. Cooling the crystal to −10°C did not improve the diffraction. Many attempts were made using other crystals from the same batch, but all gave similar highly mosaic diffraction. Finally, a well ordered diffraction pattern was obtained when a crystal from the same batch was soaked in a mixture of 75% MPD and 25% of mother liquid for two days

*To whom correspondence should be addressed

before cooling to −10°C. The crystal belonged to the orthorhombic space group $P2_12_12_1$, with unit cell parameters of a = 23.98, b = 40.77 and c = 44.84 Å and one decamer duplex in the asymmetric unit (Table 1). The unit cell is considerably shrunk compared to chimer-1 (a = 26.63, b = 45.24 and c = 47.99 Å) (1) and the volume per base pair (1,096 Å^3) is also considerably less than any of the known A-DNAs, range 1,300 ~ 1,800 A^3 (Table 2), suggesting that the present structure is not isomorphous to our earlier structure.

Three dimensional x-ray intensity data up to 1.9 Å resolution were collected at −10°C using an in-house Siemens-Nicolet area detector mounted on a four circle goniometer, with a Max-Science rotating anode operated at 50 kV and 90 mA and a graphite monochromater to isolate Cu-Kα radiation. The crystal to detector distance was 12cm. A 180° φ-scan at χ = 0°and a ω-scan at φ = 90° and χ = 45° were performed in 0.25° steps. A total of 1020 frames were collected, with an exposure time of 90 seconds per frame. The frames were processed using XENGEN 2.0 software (9). When the φ- and ω-scan data were merged, a total of 9305 reflections were obtained which yielded 2,365 unique reflections, with an R_{symm} = 5.8%. In the 8.0−1.9 Å resolution range, there were 2,314 unique reflections with F ≥ 1σ(F) which were used in the refinement.

Table 1. Crystal data and refinement parameters

Unit cell dimensions	
a (Å)	23.98
b	40.77
c	44.84
Space group	$P2_12_12_1$ orthorhombic
Molecule/asymmetric unit cell	1 duplex
Resolution range (Å)	8.0−1.9
Number of reflections (F ≥ 1σ(F)) used in refinement	2314
Final R-value (%)	14.5
RMS deviation from ideal geometry	
parameter file used	param11.dna
bond lengths	0.015 Å
bond angles	3.8°
dihedral angles	32.0°
'improper' angles	2.1°
Final model	
nucleic acid atoms	408
spermine atoms	14
water molecules	67
Average thermal parameter (Å^2)	
nucleotide	15
spermine	33
water molecules	48

Structure solution and refinement

Even though the unit cell dimensions are significantly shortened, the atomic coordinates of chimer-1 were used as a starting model in our searches. A rigid body refinement using XPLOR (10) with the 50 low resolution reflections between 25.0−8.0 Å (F ≥ 10σ(F)) dropped the R value from 56.4% to only 44.6%. However, a molecular replacement search carried out with the same starting model with translation grids of 0.48, 0.41 and 0.45 Å along the 'a', 'b' and 'c' axes, respectively, dropped the R value to 34.3% when the model was moved 1.9 Å along the 'bc' plane (Figure 1). In the subsequent refinement cycles, the resolution was extended in 0.5 Å steps to 2.5 Å and the R value was 33.4% for 1699 reflections. The omit 3Fo−2Fc and difference Fo−Fc maps clearly showed densities for the omitted residues and the O2′-hydroxyl groups. Further refinement with isotropic temperature factors for the nucleotide atoms and extending the resolution in 0.1 Å-steps from 2.5 to 1.9 Å, dropped the R value to 23.9% for 2314 reflections (F ≥ 1σ(F)). At this point, the model was annealed by initially heating the system to 4000°C and slow cooling to 300°C at 0.5fs sampling intervals using only the higher intensity data (1378 reflections with F ≥ 5σ(F)). A cycle of refinement including all reflections then dropped the R value to 21.2%. The model was refitted again into 3Fo−2Fc and Fo−Fc difference maps calculated by omitting one base pair at a time. The difference electron density map showed a continuous zig-zagging density (>3σ) in an interstitial space similar to that in spermine phosphate hexahydrate (11) (Figure 2). Fitting a spermine to this density and further refinement dropped the R value to 19.0%. At this stage, the potential solvent sites were incorporated into the model if they appeared in both the 3Fo−2Fc and Fo−Fc (at heights ≥2.0σ above the mean) electron density maps, and formed hydrogen bonds to either the polar nucleic acid atoms or other already established water molecules. In this way, 67 ordered water molecules were located and included in the refinement and the R value dropped to 15.4%. Several additional alternating cycles of refinement and model refitting dropped the R to 14.5%. The final model contains 408 nucleotide atoms, 1 spermine and 67 water molecules. The average error in the coordinates, as

Table 2. Lattice volume per base pair in spermine binding and other selected oligonucleotide crystal structures

Type	Sequence	Space group	Volume(Å^3)/ base pair	Reference
A-DNA/RNA, spermine	r(C)d(CGGCGCCG)r(G)	$P2_12_12_1$	1096	this work
A-DNA/RNA, spermine	d(GGGTATACGC)· d(CCCATAT)r(GCG)	$P2_12_12_1$	1344 1284*	19,27
A-DNA, spermine	d(GTGTACAC)	$P4_32_12$	1393	3
A-DNA, spermine	d(CCCCCGCGGGGG)	$P3_221$	1597	4
A-DNA/RNA	d(CCGGC)r(G)d(CCGG)	$P2_12_12_1$	1391	1
A-DNA/RNA	r(GCG)d(TATACGC)	$P2_12_12_1$	1300	26
A-DNA/RNA	r(G)d(CGTATACGC)	$P2_12_12_1$	1357	19
A-DNA/RNA	d(GCGT)r(A)d(TACGC)	$P2_12_12_1$	1323	19
A-DNA	d(CCCGGCCGGG)	$P2_12_12_1$	1303	20
A-DNA	d(GCGGGCCCGC)	$P2_12_12_1$	1339	25
B-DNA	d(CCGGCGCCGG)	R3	1642	2

*for −110°C data.

estimated from Luzzati plots (12), is about 0.19 Å. The rms deviation from ideality is 0.015 Å for the bond lengths, 3.8° for the bond angles and 2.1° for the 'improper' angles (Table 1). The atomic coordinates will be deposited with the Brookhaven Protein Data Bank (13).

RESULTS AND DISCUSSION

Overall structure and bending

The chimeric decamer shows a typical A-DNA/RNA conformation, with all its sugars in the C3′-*endo* puckering. The superposition of the decamer on fiber A-DNA (14) shows an rms deviation of 2.1 Å, with the terminal ribose residues deviating by about 3.0 Å, indicating that the decamer is highly bent. Local helix axis calculations, using NEWHEL92 program (R. E. Dickerson, personal communication), show that the decamer is bent by 31° at the fourth base pair G(4)·C(17) into the major groove (Figure 5), compared to the 16° bend at the same locus in chimer-1. The significant bend in the major groove constricts the P(2)−P(13) separation to 7.2 Å (Figure 4) which is stabilized by a bridging water molecule between the anionic O2P atoms of residues C(2) and G(13) (Figure 6(c)).

With respect to the local helix axis, the first four base pairs of the decamer show 10.89 residues per turn, but the last six base pairs are less wound and more extended with 11.70 residues per turn. Depending on the choice of the helix axis (15), the averaged helix parameters, namely rise (local, 3.1 vs overall, 2.4 Å) and inclination (7.9 vs 18.7°) are quite different while the twist (31.8 vs 32.4°), x-displacement (−4.0 vs −4.7 Å), roll (3.0 vs −4.2°), tilt (0.0 vs −0.8°) and tip (−0.5 vs −0.7°) show little differences. The slide (−1.6 Å), propeller twist (7.6°) and buckle (−1.3°) are independent of the choice of the helix axis.

Interaction of spermine

The packing of the bent duplexes creates an interstitial space trapping an extended spermine molecule which neutralizes the negatively charged phosphate groups (Figure 2 and 6). The four positively charged ammonium groups on spermine (at pH 7) interact with the phosphate groups either directly or via water bridges (Figure 6(b)) (Table 3). N1 of spermine is bridged to three water molecules. One of the waters is bridged by another

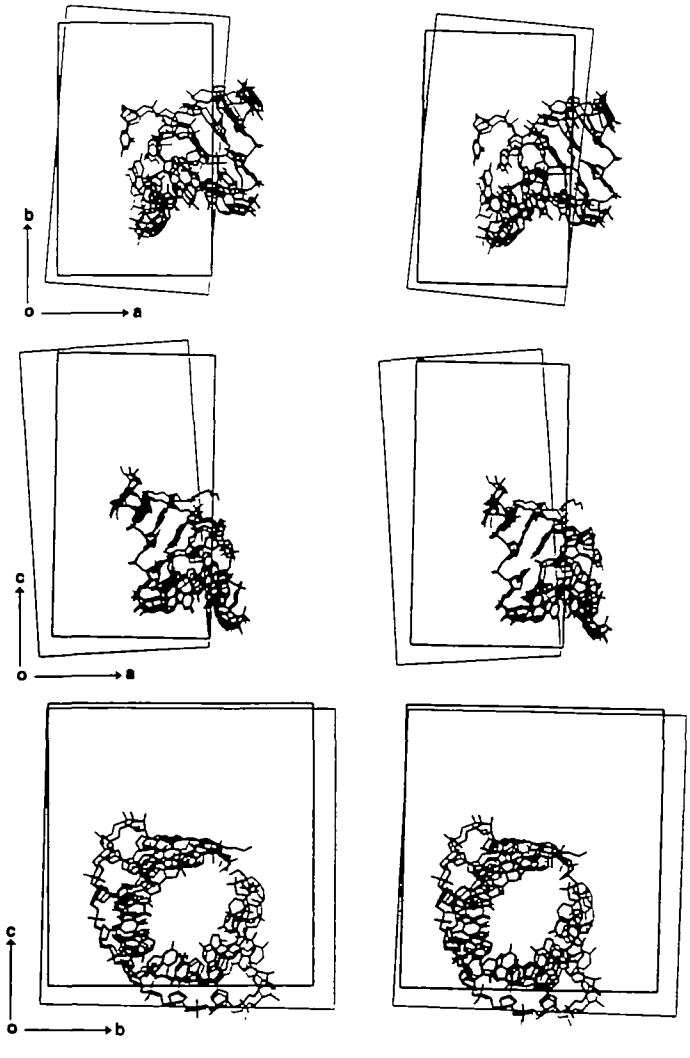

Figure 1. Stereo-view of the overlay of the duplexes in r(C)d(CGGCGCCG)r(G)·spermine (thick lines) and d(CCGGC)r(G)d(CCGG) (thin lines) showing the molecular orientation and their crystal lattices for the three different projections. The differences in the orientation of the unit cells show the degree of non-isomorphism in the two structures. Note that the duplexes in the bottom projection shows a circle for the present decamer compared to the open circle for the earlier decamer (1).

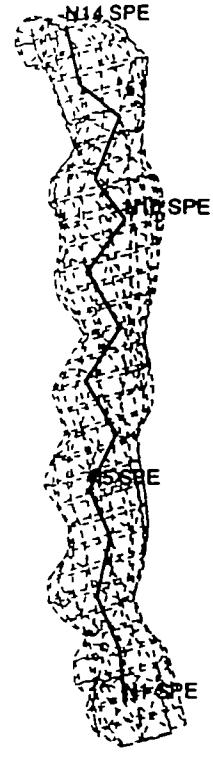

Figure 2. The omit 3Fo−2Fc electron density map (>1.5σ) showing the spermine molecule which was not included in the calculation. The zig-zagging spermine molecule is bent with a torsion angle about the C9-N10 bond of 128° (+*anticlinal*) compared to the average torsion angle of −163° (−*antiperiplanar*) for the remaining bonds. The average C-C/C-N bond length of the spermine molecule is 1.51 Å, range 1.49 ~ 1.54 Å.

water molecule to the C(12) phosphate group. The second water molecule is bridged to the G(13) phosphate group of a symmetry related duplex, while the third water molecule simply hydrates N1. N5 of spermine makes three hydrogen bonds; two directly to the phosphate groups of G(6) and G(13) of two symmetry related duplexes and the third by a water bridge to the phosphate group of C(2) and G(13) (Figure 6). N10 also forms three direct hydrogen bonds/electrostatic interactions to the phosphate groups of C(5), G(14) and G(19) of three symmetry related duplexes. N14, at the opposite end of spermine, is engaged in three hydrogen bonding and two electrostatic interactions with the phosphates of four neighboring duplexes. Two of the hydrogen

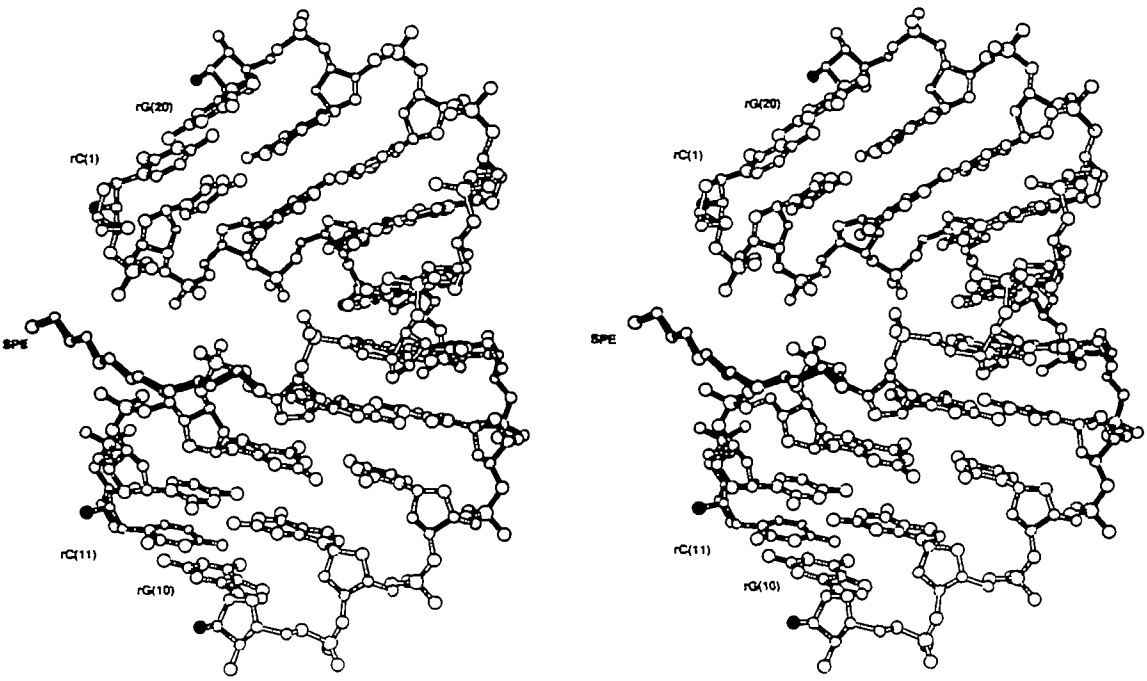

Figure 3. Stereo-view of the RNA−DNA−RNA chimeric decamer duplex (open bonds)−spermine (dark bonds) complex showing the overall structure viewed normal to the pseudo-dyad in the plane of the page. The dark atoms indicate the O2′-hydroxyl groups of the terminal ribose residues.

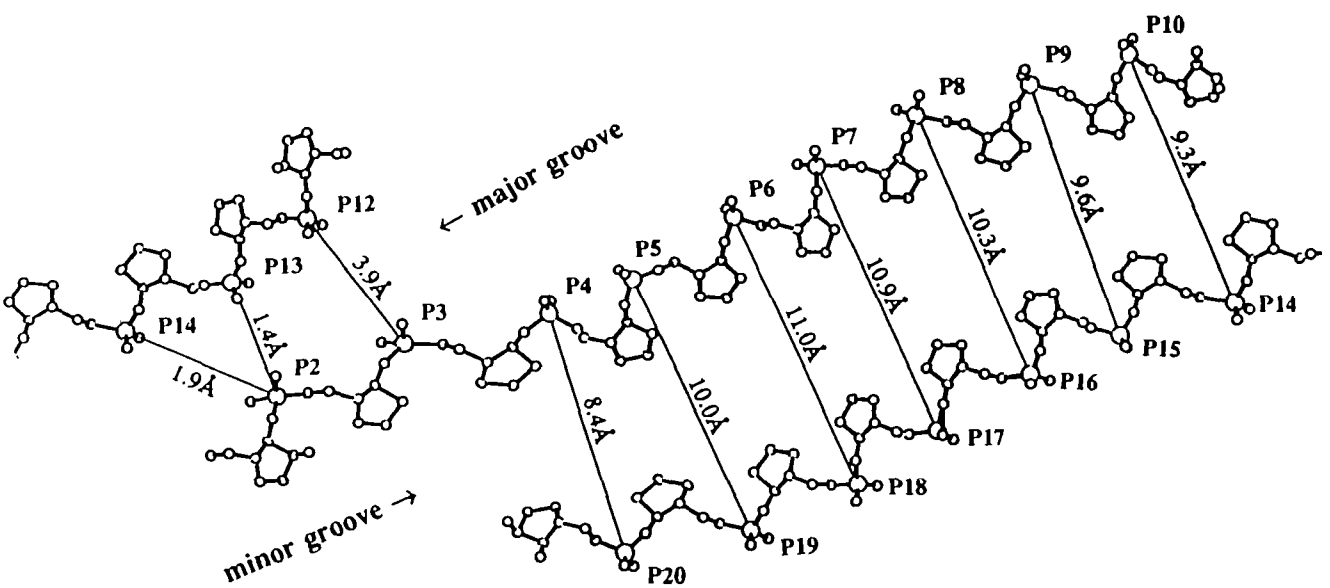

Figure 4. Cylindrical projection of the sugar-phosphate backbone of r(C)d(CGGCGCCG)r(G), computed at r of 10 Å and an angular range of 450°. The major and minor groove widths were obtained by subtracting 5.8 Å (van der Waal's radii of phosphate groups) from the P−P separation. Notice the constriction in the major groove between P2 and P13.

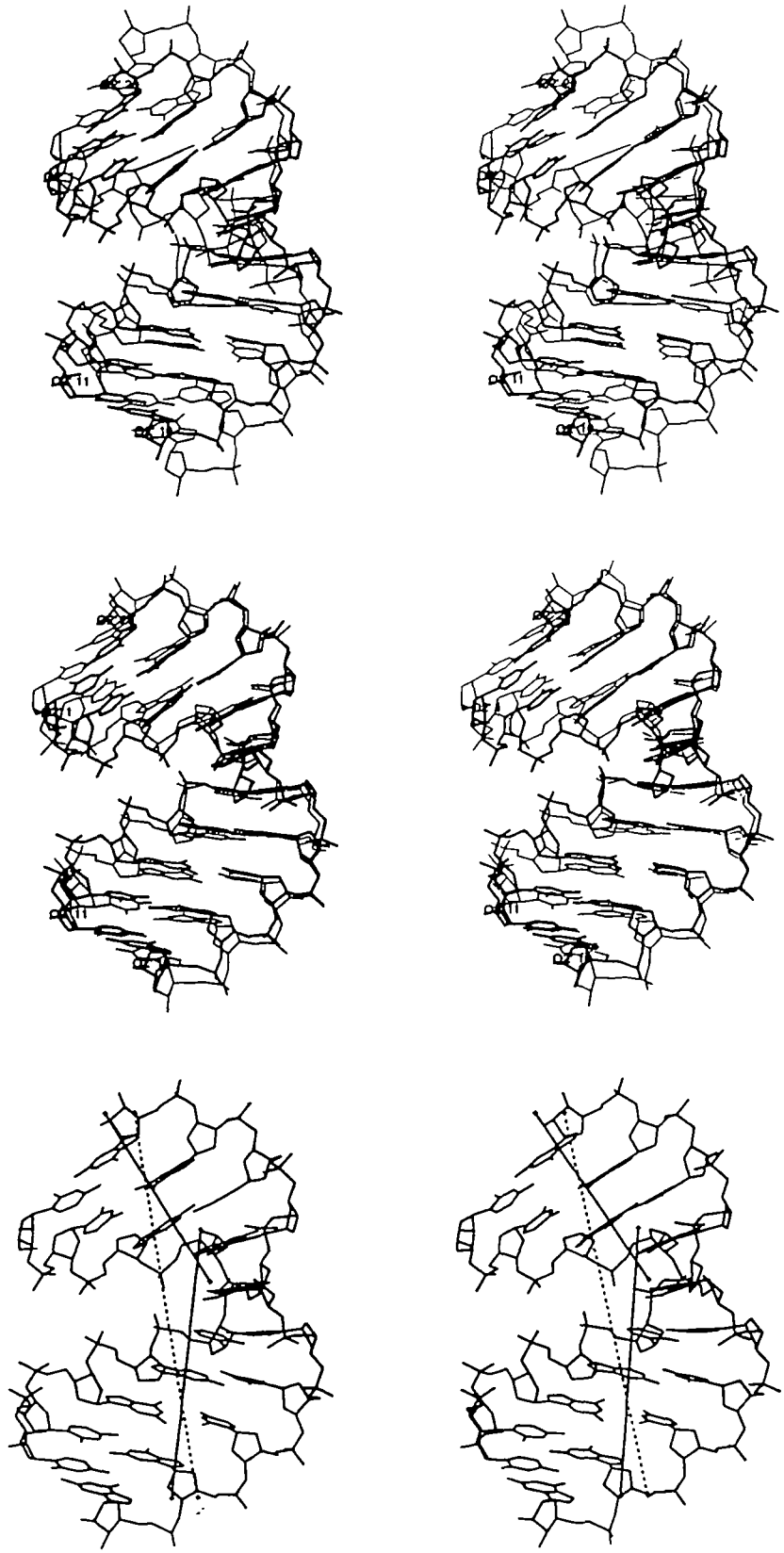

Figure 5. (**Top**) Stereo-view of the superposition of the RNA−DNA−RNA decamer r(C)d(CGGCGCCG)r(G) (thick lines) and fiber A-DNA (thin lines), overall rms deviation of 2.1 Å. (**Middle**) Stereo-view of the superposition of the present decamer (thick line) and the DNA−RNA decamer d(CCGGC)r(G)d(CCGG) (1), overall rms deviation of 1.5 Å. Note both superpositions clearly show the compression in the length as well as in the major groove of the chimer. The P−P distance between the residues C(2) and G(14) (7.7 Å) is extremely short compared to that of fiber A-DNA (10.6Å) and the DNA−RNA decamer (11.3 Å). (**Bottom**) Illustrating the 31° bend of the decamer and showing both the local (for the first 4 base pairs and the last 6 base pairs; solid-thicker lines) and global (dashed-thicker line) helix axes.

bonds are water mediated while the third is direct. Thus, the 4 phosphate groups of C(2), C(5), G(6) and rG(10) on strand 1 and the 6 phosphate groups of C(12), G(13), G(14), C(15), G(19) and rG(20) on strand 2 interact with spermine molecules. The longest consecutive stretch of phosphate groups that interacts with spermine is G(13), G(14) and C(15) on strand 2 with a cross-strand interaction to the phosphate group of C(2) on strand 1 of the same duplex.

Backbone distortion and base stacking

Even though the duplex is severely distorted and compressed, the average backbone torsion angles are within the range observed for other A-DNA crystal structures. However, when the individual torsion angles are examined (Table 4), 18 of the 20 residues show the preferred geometry (major conformation), except C(5) and G(13) which show the less favored (minor conformation) (16). The α (P-O5′) and γ (C5′-C4′) torsions of the latter residues are not exactly related by the α-γ crank-shaft motion because their β (O5′-C5′) torsions are significantly different from 180°, for C(5) β = 236° and for G(13) β = 208°. The minor conformations further show that the backbone P(5)−P(6) and P(13)−P(14) distances are 6.7 Å and 6.5 Å, respectively, and greater than the average P−P distance of 5.9 Å for the duplex. In the preferred conformation C(5) and G(13) of the two strands will generate close contacts (<2.4 Å) with symmetry related duplexes. Thus, the distorted conformations

(a)

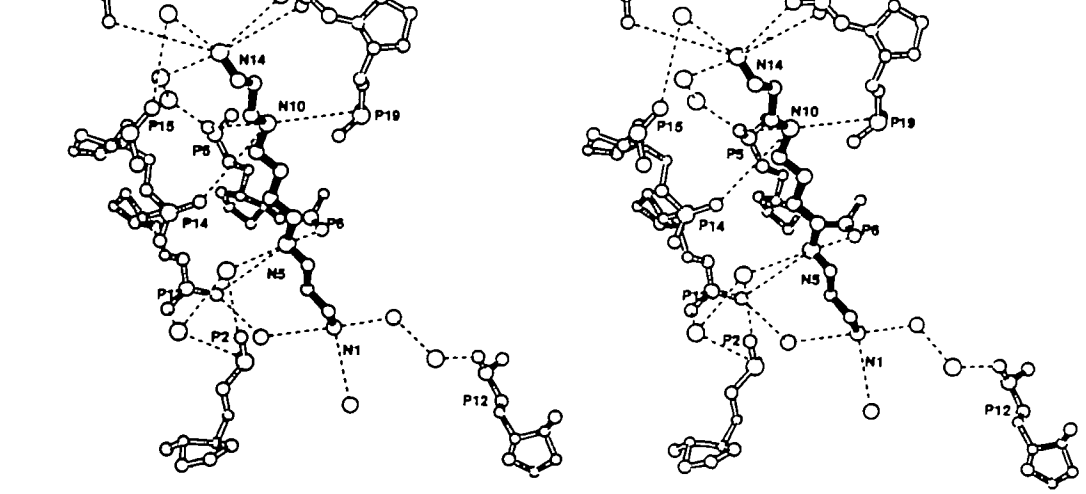

(b)

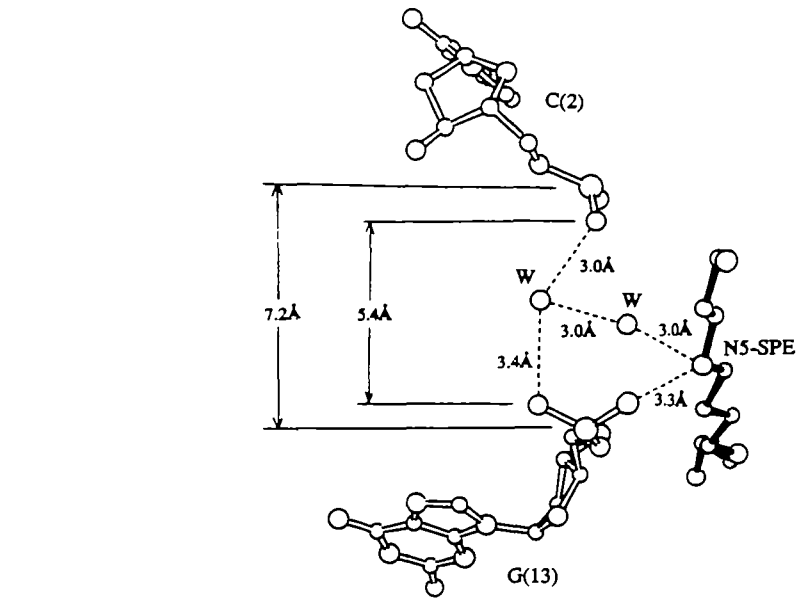

(c)

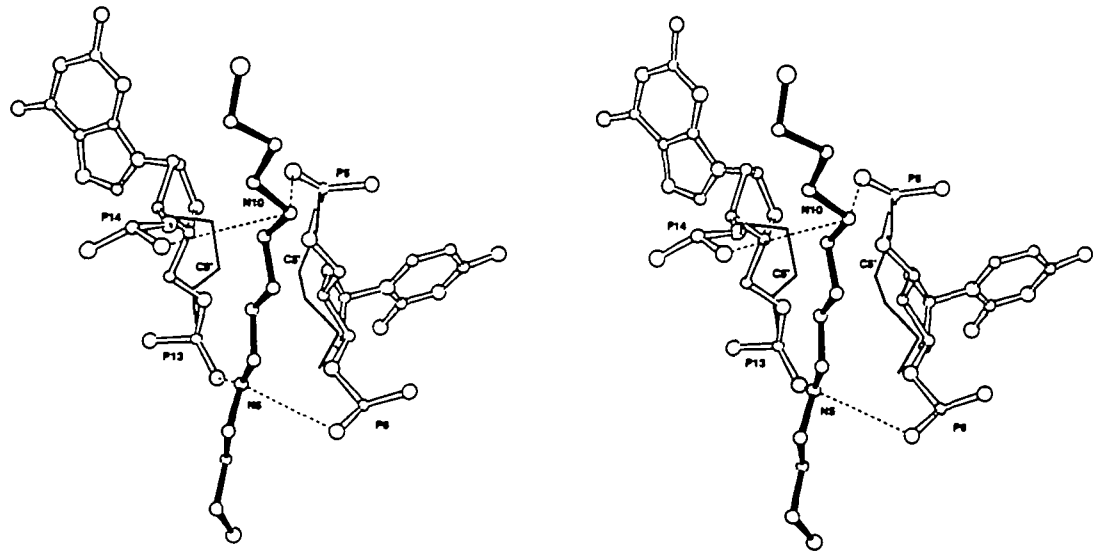

(d)

Figure 6. (a) Stereo-view of the encapsulated spermine molecule in an interstitial space formed by symmetry related duplexes. Only three of the five surrounding duplexes are shown. (b) Spermine (dark bonds) interactions with the phosphate groups (open bonds) of the five symmetry related duplexes. (c) Cross-strand spermine interaction. Residues C(2), G(13), G(14) and C(15) are from the same duplex with the cross-strand interactions. (d) An overlay of the distorted backbone of C(5) and G(13) (open bonds) on the preferred backbone (solid lines). Note the short contact (2.4 Å) for C5′ atoms in the normal backbone and interaction of the phosphate groups with the spermine molecule (dashed lines).

are probably adopted to avoid the steric clash (Figure 6(d)). It appears that the observed distortions arise from the spermine molecule compacting the DNAs .

The base stacking patterns are similar to those of other A-DNA structures, except for the G(4)pC(5) step which is distorted at the C(5) backbone. The stacking of the G(4) and C(5) bases in the top half of the duplex is better compared to that of the complementary C(17) and G(16) bases (Figure 7 (top)). In contrast, the pseudo-dyad related G(14)pC(15) step of the bottom half of the duplex shows the opposite base stacking pattern: poor stacking for the purine−pyrimidine G(14)pC(15) step and good stacking for the complementary pyrimidine−purine C(7)pG(6) step. This is probably due to the sliding of the base plate G(4)·C(17) towards the minor groove leading to a break down in the molecular dyad of the duplex. Also, this facilitates the N2 and N3 atoms of G(4) and the O2 atom of C(17) to form hydrogen

bonds with the neighboring molecule. Even though the residue G(13) of the bottom half of the duplex also shows the distorted backbone conformation, the base stacking of the C(12)pG(13) step shows very similar pattern to the pseudo-dyad related C(2)pG(3) step (Figure 7 (bottom)). Thus, the distorted backbone conformation of both strands is not correlated with the base stacking (17).

Tertiary base-paired multiples

To date three kinds of minor groove tertiary base-paired multiples have been found, all involving G·C base pairs. We call a base-paired multiple (a) a base-paired triple when the guanine N2 and N3 atoms of a G·C base pair are hydrogen bonded to a neighboring G·C base pair across the O2 and N2 atoms so that all three bases [G*(G·C)] interact with each other and (b) a base-paired quadruple when all four bases are involved in the tertiary base pairing and forming two N2 ··· O2 hydrogen bonds. When only the guanines of two G·C base pairs of neighboring molecules interact to form a G·G base pair through the N3 and N2 atoms as in the Drew-Dickerson's B-DNA dodecamer (18), we refer to this as a quasi base-paired triple (c). Notice that the two G·C base pairs are disposed in the same direction in (a), but in opposite directions in (b) and (c). The present decamer shows three base-paired triples, (C(18)·G(3))*rG(10), G(4)*(rG(10)·rC(11)) and (C(7)·G(14))*rG(20), and one base-paired quadruple, (G(6)·C(15))*(rC(1)·rG(20)) (Figure 8). All of these base-paired multiples are found in chimer-1. The base-paired quadruple was also found in the top half of the chimeric decamer

Table 3. Hydrogen bonding and electrostatic interactions of spermine

Atom1/ Spermine	Distance (Å)	Atom2/ Residue	Distance (Å)	Atom3/ Residue	Distance (Å)	Atom4/ Residue
N1	2.8	W52	3.2	O2P-G(13)	–	–
	2.8	W56	3.1	W45	3.3	O2P-C(12)
	2.8	W87	–	–	–	–
N5	3.3	O2P-G(6)	–	–	–	–
	3.3	O2P-G(13)	–	–	–	–
	3.0	W46	–	–	–	–
			3.0	W67	3.0	O2P-C(2)
					3.4	O1P-G(13)
N10	3.6	O2P-C(5)	–	–	–	–
	3.8	O2P-G(14)	–	–	–	–
	3.3	O2P-G(19)	–	–	–	–
N14	2.5	W29	3.4	W55	2.8	O2P-C(5)
	3.7	O2P-rG(10)	–	–	–	–
	2.6	W33	2.7	O2P-C(15)	–	–
	2.8	O1P-rG(20)	–	–	–	–
	3.5	O2P-rG(20)	–	–	–	–

Table 4. Backbone torsion angles*, sugar-base glycosyl torsion angles (χ) and pseudorotation phase angles (P)

Sequence	α	β	γ	δ	ϵ	ζ	χ	P
rC(1)	–	–	59°	78°	205°	288°	198°	13°
C(2)	299°	156°	55	82	185	296	196	16
G(3)	302	147	61	87	185	282	204	20
G(4)	280	200	53	77	197	292	216	11
C(5)	104	236	199	78	215	282	196	4
G(6)	265	189	66	75	226	283	201	14
C(7)	304	156	54	76	199	290	207	14
C(8)	293	161	67	69	206	272	190	20
G(9)	299	160	66	72	215	283	188	9
rG(10)	284	200	69	82	–	–	207	5
rC(11)	–	–	59	78	214	290	201	8
C(12)	290	180	62	76	174	299	208	15
G(13)	120	208	197	82	210	295	181	−1
G(14)	295	165	91	79	207	282	198	11
C(15)	291	175	59	81	209	309	208	−3
G(16)	297	149	64	86	207	276	196	22
C(17)	294	149	56	76	231	279	198	6
C(18)	305	157	68	75	196	283	197	32
G(19)	303	158	63	75	194	291	187	27
rG(20)	296	187	50	84	–	–	213	20
AV	291#	168#	61#	77	204	287	200	13
RMS	30	19	15	5	14	9	9	9

*The IUPAC-IUB (28) backbone torsion angles are O3′-P-α-*O5′*-β-C5′-γ-C4′-δ-C3′-ϵ-O3′-ζ-P- O5′. An earlier definition which still used for the corresponding backbone torsion angles are ω, ϕ, ψ, ψ', ϕ' and ω', respectively (29).
#The α, β, and γ values of the residues C(5) and G(13) were excluded in the calculation of the average values.

d(GCGT)r(A)d(TACGC) (19) and the base-paired triples in the A-DNA decamer d(CCCGGCCGGG) (20) and the bottom half of the A-DNA dodecamer d(CCCCCGCGGGGG) (4). The top half of the latter also shows a quasi base-paired triple as in the B-DNA dodecamer (18). All of the above base-paired multiples occur in the minor groove, in contrast to the major groove interactions in triple helices (21) and t-RNA^{Phe} (22–24).

Ribose 2′-hydroxyl groups

The ribose 2′-hydroxyl groups in the minor groove hydrogen bond to the four base multiples. Those of 3′-terminal rG(10) and rC(11) are hydrogen bonded to N3 (2.7 Å) of G(3) and O2 (3.0 Å) of C(17), respectively (Figure 8 (a)). The 2′-hydroxyl groups of 5′-terminal rC(1) and rG(20) residues form hydrogen bonds with N2 (3.2 Å) and N3 (3.2 Å) of G(6) and N3 (2.8 Å) of G(14), respectively, (Figure 8(b)). These hydrogen bonding interactions further contribute to the stability of the base-paired multiples. Although all four 2′-hydroxyl groups have similar intermolecular hydrogen bonds, the environments differ depending on whether they are on the 5′- or the 3′-termini. The 2′-hydroxyl groups of the 5′-terminal rC(1) and rC(11) form hydrogen bonding interactions with the minor groove atoms of a symmetry related molecule with solvent accessibilities of 9.5 Å^2 for rC(1) and 10.3 Å^2 for rC(11). In contrast, the 2′-hydroxyl groups of the 3′-terminal rG(10) and rG(20) are screened by a symmetry related molecule and have no solvent accessibility. This difference in the hydrogen bonding and contacts with the neighboring molecules is probably due to the asymmetric bending of the duplex.

CONCLUSION

The decamer duplex could have assumed a mixed conformation where only the terminal RNA base pairs are in the preferred C3′-*endo* (A-RNA) sugar puckering, while the remaining eight inner deoxy-nucleotide residues are in the C2′-*endo* (B-DNA) puckering. This appears possible since C2′-*endo* conformation has been found for the penultimate or terminal residues of A-DNA crystal structures (17, 19). However, all the sugars were C3′-*endo* puckered. Circular dichroism studies on this chimer (data not shown) clearly show that in solution its conformation is very similar to that found in the crystal and the all-ribose A-RNA decamer r(CCGGCGCCGG) in solution.

The interstitial pocket occupied by spermine in this structure is smaller than in the other related orthorhombic $P2_12_12_1$ A-DNA decamer structures (1, 19, 20, 25–27). The chimeric decamer d(GGGTATACGC)·d(CCCATAT)r(GCG) shows only 4.4% shrinkage upon cooling to −110°C (19). In this and other known crystal structures, spermine interacts with either only the base or with both base and phosphate. Thus, spermine is not fully

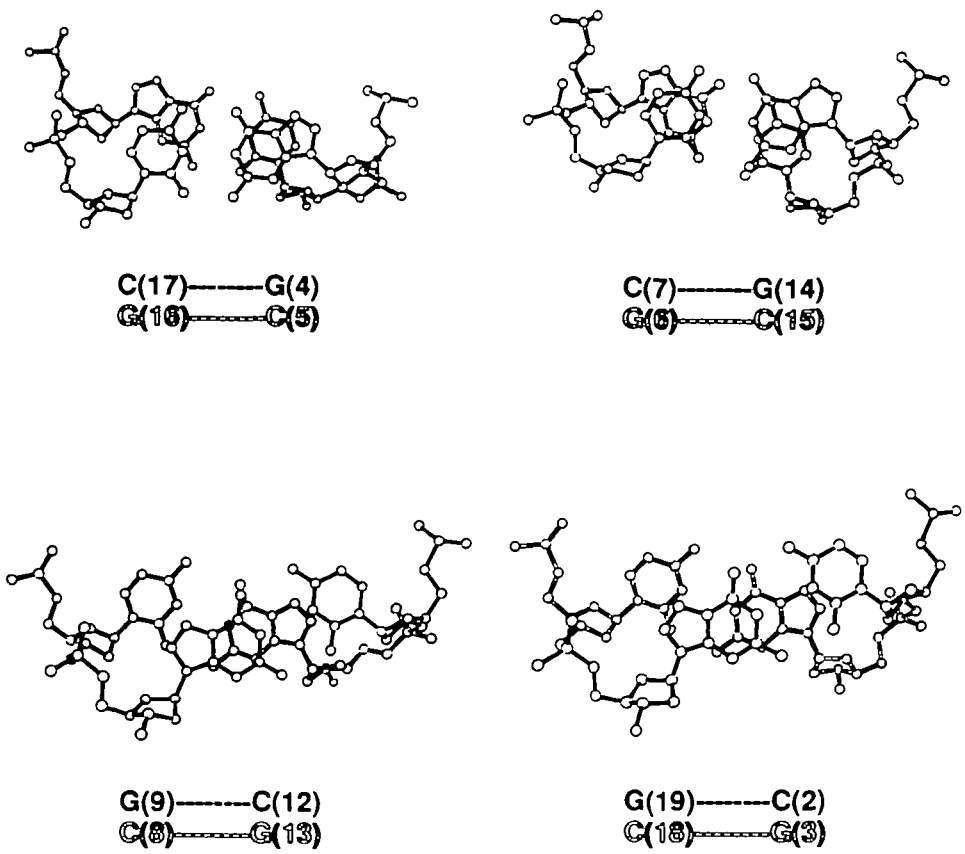

Figure 7. (Top) The base stacking pattern of the step G(4)pC(5) (left) compared to the pseudo-dyad related step G(14)pC(15) (right) (**Bottom**) The C(12)pG(13) step compared to the pseudo-dyad related C(2)pG(3) step. Note that C(5) and G(13) have the highly distorted backbone conformations for α ($+g$) and γ (t) torsions. In the top figures, the base pair G(4)·C(17) is shifted towards the minor groove of the duplex compared to the pseudo-dyad related base pair C(7)·G(14), but such a shift is not severe in the base pair G(9)·C(12) (bottom).

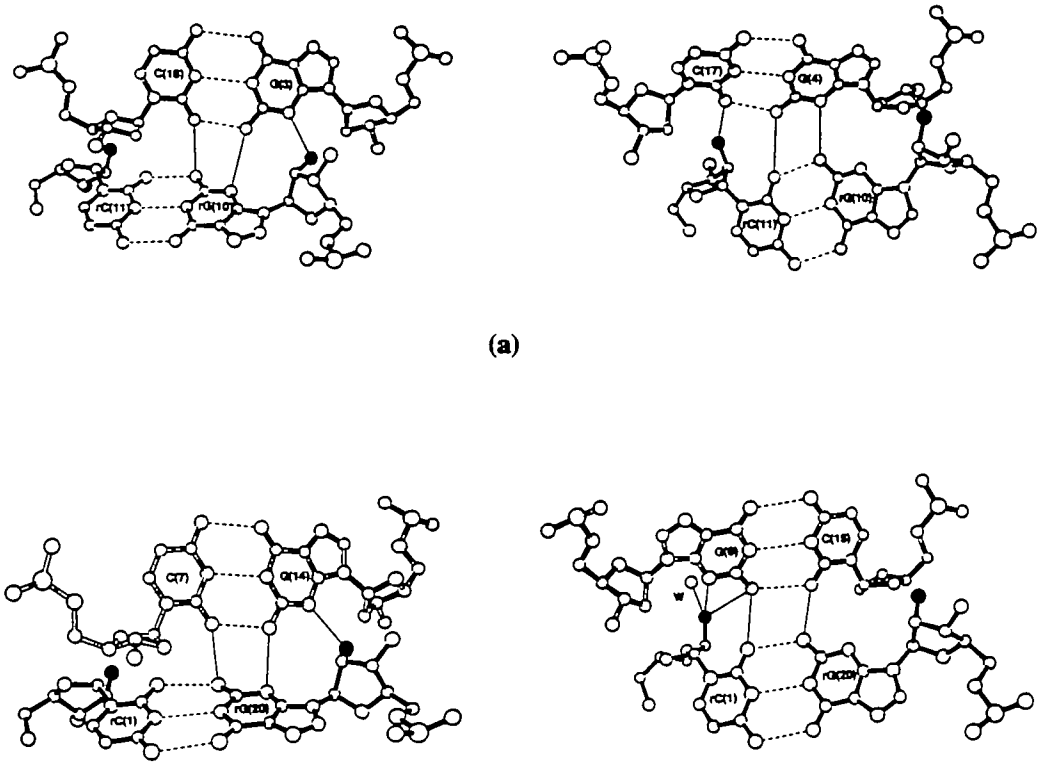

Figure 8. The tertiary base-paired multiples and the environment of the 2'-hydroxyl groups (dark circles) of the terminal ribose residues. Note that the figures are not stereo. (a) The top half of the duplex displays the two base-paired triples (C(18)·G(3))*rG(10) (left) and G(4)*(rG(10)·rC(11)) (right). Note that the base pair C(18)·G(3) is inclined at an angle of 127° with rG(10). The angle between the G(4) and the base pair rG(10)·rC(11) is 126°. The 2-amino group of the common base rG(10) in the double base-paired triple forms a bifurcated hydrogen bond. The 2'-hydroxyl groups of rG(10) and rC(11) are hydrogen bonded to N3 of G(3) and O2 of C(17) of a symmetry related duplex, respectively. (b) The bottom half of the duplex displays a base-paired triple (C(7)·G(14))*rG(20) (left) and a base-paired quadruple (G(6)·C(15))*(rC(1)·rG(20)) (right). The base pair C(7)·G(14) is inclined at an angle of 118° with rG(20) while the base pairs G(6)·C(15) and rC(1)·rG(20) are inclined at 116°. Similar to rG(10), N2 of rG(20) also forms a bifurcated hydrogen bond to the O2 atoms of C(7) and C(15). The 2'-hydroxyl group of rG(20) forms hydrogen bond with N3 of G(14) of a symmetry related duplex and that of rC(11) hydrogen bonds to N2 and N3 of G(6) and a water molecule.

involved in the direct charge neutralization of the phosphate groups and the volume per base pair in these crystals ranges from 1,300 to 1,800 Å^3 (Table 2). However, the present structure has the lowest volume per base pair (1,093 Å^3) among the known right-handed oligonucleotide crystal structures. The spermine molecule in the interstitial space is in the fully extended conformation interacting with ten phosphate groups belonging to five different surrounding duplexes. Therefore, most of the shrinkage (~25%) in the unit cell is probably caused by the ordered spermine molecule drawing the duplexes closer together and not by the cooling (−10°C) and MPD treatment of the crystal. Such extensive spermine-phosphate contacts are probably important in the condensation of nucleic acids.

ACKNOWLEDGEMENTS

We thank the National Institutes of Health of the United States Public Health Service for supporting this work through a grant GM-17378 and the Ohio State Supercomputer Center for granting time on Cray Y-MP/864.

REFERENCES

1. Ban, C., Ramakrishnan, B., and Sundaralingam, M. (1994) *J. Mol. Biol.* **235** 275–285.
2. Heinemann, U., Alings, C., and Bansal, M. (1992) *EMBO J.* **11**, 1931–1939.
3. Jain, S., Zon, G., and Sundaralingam, M. (1989) *Biochemistry* **28**, 2361–2364.
4. Verdaguer, N., Aymami, J., Fernandez-Forner, D., Fita, I., Coll, M., Huynh-Dinh, T., Igolen, J., and Subirana, J. A. (1991) *J. Mol. Biol.* **221**, 623–635.
5. Frederick, C. A., Williams, L. D., Ughetto, G., van der Marel, G. A., van Boom, J. H., Rich, A., and Wang, A. H. -J. (1990) *Biochemistry* **29**, 2538–2549.
6. Williams, L. D., Frederick, C. A., Ughetto, G., and Rich, A. (1990) *Nucleic Acids Res.* **18**, 5533–5541.
7. Egli, M., Williams, L. D., Gao, Q., and Rich, A. (1991) *Biochemistry* **30**, 11388–11402.
8. Bancroft, D., Williams. L. D., Rich, A., and Egli, M. (1994) *Biochemistry* **33**,1073–1086.
9. Howard, A. J. (1990) *XENGEN manual.* **v2.1**, Genex Corporation, Gaithersburg, MD.
10. Brunger, A. T. (1990) *XPLOR manual*, **v2.1**, Yale University, New Haven, CT.

11. Iitaka, Y., and Huse, Y. (1965) *Acta Cryst.* **18**, 110–121.
12. Luzzati, P. V. (1952) *Acta Cryst.* **5**, 802–810.
13. Bernstein, F. C., Koetzle, T. F., Williams, G. J. B., Meyer, E F. Jr., Brice, M. D., Rodgers, J. R., Kennard, O., Shimanouchi, T., and Tasumi, M (1977) *J. Mol. Biol.* **112**, 535–542
14. Chandrasekaran, R., Wang, M., Tang, M. -K., He, R. -G., Puigianer, L. C., Byler, M. A., Millane, R P., and Arnott, S (1989) *J. Biomol. Struct. Dynam.* **6**, 1189–1202.
15. Bingman, C. A., Zon, G., and Sundaralingam, M. (1992) *J. Mol. Biol.* **227**, 738–756.
16. Sundaralingam, M., and Ban, C. (1994) The Asian Region Seminar on Crystallography in Molecular Biology. In *Oligonucleotides with Complementary and Non-complementary Base Pairing and Their Ligand Complexes — Major and Minor Nucleotide Conformations*. Held in University of Madras, Madras, India, December 9–4, 1993, (in press).
17. Jain, S., Zon, G., and Sundaralingam, M. (1991) *Biochemistry* **30**, 3567–3576.
18. Drew, H. R., Wang, R. M., Takano, T , Broka, C., Tanaka, S., Itakura, k., and Dickerson, R. E. (1981) *Proc Natl. Acad. U. S. A.* **78**, 2179–2183.
19. Egli, M., Usman, N., and Rich, A. (1993) *Biochemistry* **32**, 3221–3237
20. Ramakrishnan, B., and Sundaralingam, M. (1993) *J Mol. Biol.* **231**, 431–444.
21. Felsenfeld, D., Davies, D. R., and Rich, A. (1957) *J A. Chem. Soc.* **79**, 2023–2029.
22. Kim, S.-H., Suddath, F. L., Quigley, G. J, McPherson, A., Sussman, J. L., Wang, A. H. J., Seeman, N. C., and Rich, A. (1974) *Science* **185**, 435–440.
23. Klug, A., Ladner, J., and Robertus, J. D. (1974) *J. Mol. Biol.* **89**, 511–516
24. Brennan, T., and Sundaralingam M. (1975) Discussion of paper of R. G. Shulman. In *structure and conformation of nucleic acids and protein-nucleic acid interaction.* (ed. M. Sundaralingam and S. T. Rao), p165, University Park Press, Baltimore, MD.
25. Ramakrishnan, B., and Sundaralingam, M. (1993) *Biochemistry* **32**, 11458–11468.
26. Wang, A. H. -J., Fujii, S., van Boom, J. J., van der Marel, G. A., van Boeckel, S. A A., and Rich, A. (1982) *Science* **299**, 601–604.
27. Egli, M., Usman, N., Zhang, S., and Rich, A. (1992) *Proc. Natl. Acad. Sci. U.S.A.* **89**, 534–538.
28. IUPAC-IUB, (1983) *Eur. J. Biochem.* **131**, 9–15.
29. Sundaralingam, M. (1969) *Biopolymers* **12**, 297–314.